JOURNAL OF COMPUTATIONAL PHYSICS 36, 313–326 (1980)

A Finite-Element Method for Incompressible Non-Newtonian Flows

MICHEL BERCOVIER

School of Applied Science and Technology, Hebrew University, Givat Ram, Jerusalem, Israel

AND

MICHAEL ENGELMAN

Institute of Mathematics, Hebrew University, Givat Ram, Jerusalem, Israel

Received April 16, 1979; revised September 24, 1979

The extension to non-Newtonian viscous incompressible fluid flows of a finite-element method using a nine-node isoparametric Langrangian element with a penalty approach for the continuity equation is studied. The Bingham fluid is used to illustrate the effectiveness of the approach. An application to limit load analysis is also considered.

INTRODUCTION

In this paper we study the extension of an application of the finite-element method (FEM) developed for viscous incompressible flows by Bercovier and Engelman [3] to the numerical simulation of non-Newtonian incompressible flows. We shall assume that the reader is familiar with the theory and method as presented in [3]. Briefly this was as follows: the weak variational formulation of the Navier–Stokes problem was replaced by a penalty function approach for the continuity equation and it was shown that the nine-node Lagrangian isoparametric element is a powerful element when used with the penalty and reduced integration approach.

Our aim here is to study the implementation of this same penalty function approach to a class of non-Newtonian fluids. As the representative model of this class we have chosen Bingham's fluid; though the FEM presented here (and the corresponding code) is currently being used with success to study a range of non-Newtonian fluids having constitutive relations of the same type as that of Bingham's fluid, e.g., monotone perturbations [7] and blood flow simulation [8].

The advantage of a Bingham model, apart from its being representative of a large class of fluids is that it has been the subject of some mathematical studies (cf. Duvaut and Lions [5]) so that the penalty method can be theoretically justified.

Similar numerical studies have been carried out by Fortin [9] and Begis [1] using different approaches. Fortin used triangular finite elements and duality type methods. Non-Newtonian fluids together with a penalty approach were first considered by Zienkiewicz and Godbole [13] using the eight-node serendipity element.

0021-9991/80/090313–14$02.00/0

CONSTITUTIVE RELATIONS

In order to simplify the ensuing theory we will assume that thermal effects are negligible and limit ourselves to a homogeneous isotropic fluid in two dimensions. Let Ω be a bounded domain of R_2, Γ its boundary. For a given "source" field $\mathbf{f}$ we consider a fluid in motion, the appropriate equations being:
Equation of motion:

$$\rho \frac{\partial u_i}{\partial t} + u_j u_{i,j} = f_i + \sigma_{ij,j} \qquad \text{in } \Omega. \tag{1}$$

Continuity equation:

$$u_{i,i} = 0. \tag{2}$$

Boundary condition:

$$u_i |_\Gamma = 0. \tag{3}$$

The stress tensor, σ_{ij}, is given by

$$\sigma_{ij} = -p\delta_{ij} + \tau_{ij}, \tag{4}$$

P being the hydrostatic pressure and τ_{ij} the deviatoric part of the stress tensor.
We denote by D_{ij} the strain rate tensor

$$D_{ij} = \tfrac{1}{2}(u_{i,j} + u_{j,i}) \qquad u_i \text{ the velocity field of the fluid} \tag{5}$$

and by D_{II}, the second invariant of the tensor D_{ij}, given by $D_{II} = D_{ij}D_{ij}$. Similarly we define $\tau_{II} = \tau_{ij}\tau_{ij}$
We consider constitutive relations of the form

$$\tau_{ij} = 2\mu(D_{II})\, D_{ij}, \tag{6}$$

where μ is a function of D_{II} and reduces to $\mu = \mu_0$ (constant) for the Newtonian case. More precisely, for fluids exhibiting rigid visco-plastic behavior we have

$$\begin{aligned} &\tau_{ij} = 2\mu(D_{II})\, D_{ij} && \text{if} \quad \tau_{II} \geqslant g^2, \\ &D_{ij} = 0 && \text{if} \quad \tau_{II} < g^2, \end{aligned} \tag{7}$$

where g is a constant called the plasticity level.

As stated previously we will limit ourselves to a discussion of Bingham's fluid for which the constitutive relation is

$$\begin{aligned} &\tau_{ij} = 2\mu_0 D_{ij} + g D_{ij}/D_{II}^{1/2} && \text{if} \quad \tau_{II} \geqslant g^2, \\ &D_{ij} = 0 && \text{if} \quad \tau_{II} < g^2, \end{aligned} \tag{8}$$

i.e.,

$$\mu(D_{II}) = \mu_0 + (g/2)\, D_{II}^{-1/2}, \qquad \tau_{II} \geqslant g^2. \tag{9}$$

It is clear that τ_{ij} is not defined if $D_{II} = 0$ and that this may lead to numerical difficulties if (8) or (9) is used. One way to overcome this difficulty is to replace (9) by

$$\mu_\eta(D_{II}) = \mu_0 + (g/2)(D_{II} + \eta)^{-1/2}, \tag{10}$$

where η can be as small as one wishes. Equation (10) actually leads to a weak formulation of Eqs. (1)–(4). Finally we limit ourselves to the stationary case; extension to time-dependent problems is straightforward.

Weak Formulation

We introduce the Sobolev spaces

$$H_0^1(\Omega) = \{\mathbf{u} \in L^2(\Omega)\colon \mathbf{u}_i \in L^2(\Omega),\ \mathbf{u}\,|_\Gamma = 0\},$$
$$V = (H_0^1(\Omega))^2,$$
$$W = L^2(\Omega)/R$$

and define the following bilinear and trilinear forms on $V \times V$ and $V \times V \times V$, respectively, given by $Re = \mu_0/\rho LV$, where L and V are, respectively, a characteristic length and a characteristic velocity of the flow and μ_0 is as in Eq. (9).

$$a(\mathbf{u}, \mathbf{v}) = \int_\Omega D_{ij}(\mathbf{u})\, D_{ij}(\mathbf{v})\, d\Omega,$$
$$b(\mathbf{u}, \mathbf{v}, \mathbf{w}) = \int_\Omega u_i v_{j,i} w_j\, d\Omega,$$

and

$$\hat{b}(\mathbf{u}, \mathbf{v}, \mathbf{w}) = \tfrac{1}{2}[b(\mathbf{u}, \mathbf{v}, \mathbf{w}) - b(\mathbf{u}, \mathbf{w}, \mathbf{v})].$$

It can be shown [5] that if there is a regular solution of (1), (2), (3), and (10) (we assume for simplicity $\rho \equiv 1$) then this solution is also a solution of the following problem: find $(\mathbf{u}, p) \in V \times W$ so that

$$\frac{1}{Re}\, a(\mathbf{u}, \mathbf{v}) + \hat{b}(\mathbf{u}, \mathbf{u}, \mathbf{v}) + \frac{g}{Re} \int_\Omega \frac{D_{ij}(\mathbf{u})\, D_{ij}(\mathbf{v})}{(D_{II} + \eta^2)^{1/2}}\, d\Omega + \int_\Omega P \operatorname{div} \mathbf{v}\, d\Omega = \int_\Omega \mathbf{f} \cdot \mathbf{v}\, d\Omega$$
$$\operatorname{div} \mathbf{u} = 0 \qquad \text{for all} \quad \mathbf{v} \in V. \tag{11}$$

Equation (11) is dimensionless; Re is the Reynolds number.

Rigorously we must denote a solution of (10) as $(\mathbf{u}_\eta, P_\eta)$ because of its dependence

on η. Duvaut and Lions [5] have shown that for Re small enough $(\mathbf{u}_\eta, P_\eta)$ is unique and $\mathbf{u}_\eta$ tends weakly in V to $\mathbf{u}^*$, the unique solution of the inequality:

$$\frac{1}{Re}\, a(\mathbf{u}, \mathbf{v} - \mathbf{u}) + \hat{b}(\mathbf{u}, \mathbf{u}, \mathbf{v}) + \frac{g}{Re}\int_\Omega D_{II}^{1/2}(\mathbf{v}) - \frac{g}{Re}\int_\Omega D_{II}^{1/2}(\mathbf{u}) \geqslant \int_n \mathbf{f}\cdot(\mathbf{v} - \mathbf{u})\, d\Omega$$
$$\text{for all } \mathbf{v} \in V \text{ such that } \operatorname{div} \mathbf{v} = 0. \tag{12}$$

Since in the FEM formulation we actually define (11) and (12) on a finite-dimensional subspace $V_n \subset V$ the computed solution $\mathbf{u}_n$ of (11) will always converge strongly to the solution $\mathbf{u}^*$ of (12) in V_n.

In practice, one takes η as small as possible. Note that a priori there is no unique "hydrostatic pressure" corresponding to the solution of (12).

Penalty Function Approach

In order to overcome the numerical problems arising from the continuity equation (2) we proceed as in [3] and replace (11) by

$$\frac{1}{Re}\, a(\mathbf{u}_\epsilon, \mathbf{v}) + \hat{b}(\mathbf{u}_\epsilon, \mathbf{u}_\epsilon, \mathbf{v}) + \frac{g}{Re}\int_\Omega \frac{D_{ij}(\mathbf{u}_\epsilon)\, D_{ij}(\mathbf{v})}{(D_{II}(\mathbf{u}_\epsilon) + \eta^2)^{1/2}}\, d\Omega$$
$$\times \frac{1}{\epsilon}\int (\operatorname{div} \mathbf{u}_\epsilon)(\operatorname{div} \mathbf{v})\, dV = \int_\Omega \mathbf{f}\cdot\mathbf{v}\, d\Omega \tag{13}$$

and (12) by

$$\frac{1}{Re}\, a(\mathbf{u}_\epsilon, \mathbf{v} - \mathbf{u}_\epsilon) + \hat{b}(\mathbf{u}_\epsilon, \mathbf{u}_\epsilon, \mathbf{v}) + \frac{g}{Re}\int_\Omega D_{II}^{1/2}(\mathbf{v}) - \frac{g}{Re}\int_\Omega D_{II}(\mathbf{u}_\epsilon)\, d\Omega$$
$$\geqslant \int_\Omega \mathbf{f}\cdot(\mathbf{v} - \mathbf{u}_\epsilon)\, d\Omega \tag{14}$$

Then for Re "small enough" we have the following error estimate.

Theorem. *Let* $\mathbf{u}_{\eta,\epsilon}$ (*resp.* $\mathbf{u}_\epsilon$) *be the unique solution of* (13) (*resp.* (14)) *and let* $\mathbf{u}_\eta$ (*resp.* $\mathbf{u}$) *be the unique solution of* (11) (*resp.* 12); *then*

$$\| \mathbf{u}_\eta - \mathbf{u}_{\eta,\epsilon} \| \leqslant c\epsilon^{1/2}$$
and
$$\| \mathbf{u} - \mathbf{u}_\epsilon \| \leqslant c'\epsilon^{1/2}. \tag{15}$$

For proof cf. [2]. Note that compared with the similar result for the Newtonian case [3] we have an error estimate of $O(\epsilon^{1/2})$ instead of $O(\epsilon)$. The proof of estimate (15) is a consequence of the classic property (cf. [11])

$$\sup_{\mathbf{v}\in V-\{0\}} \frac{\int_\Omega P \operatorname{div} \mathbf{v}\, d\Omega}{\| \mathbf{v} \|_V} \geqslant k \| P \|_W \qquad \text{for all } P \in W. \tag{16}$$

In order to obtain a discrete analog of (15) it is then crucial to have an FEM such that (16) is satisfied. As stated in [3] and proved in [6] this is the case for the nine-node Langrangian element provided that the continuity equation be satisfied in a weaker sense, which we denote by $\operatorname{div}_h \mathbf{u} = 0$. For full details of this definition we refer the reader to [3]. This definition amounts to a "reduced" integration for the penalty term $\int_\Omega (\operatorname{div} \mathbf{u}_\epsilon)(\operatorname{div} \mathbf{v})\, d\Omega$ in (13).

Finite-Element Implementation and Solution Algorithm

We designate by V_h the finite-dimensional space defined by a given FEM "triangulation" and the corresponding basis functions derived from the nine-node Lagrangian element. Problem (11) is nonlinear; in order to solve it over V_h we use the following quasi-linearization algorithm. Let $\mathbf{u}^0$ be an initial guess, $\mathbf{u}^n$ the nth iterate; then we compute $\mathbf{u}^{n+1}$, the solution of

$$\frac{1}{Re}\, a(\mathbf{u}^{n+1}, \mathbf{v}) + \hat{b}(\mathbf{u}^n, \mathbf{u}^{n+1}, \mathbf{v}_h) + \frac{1}{\epsilon}(\operatorname{div}_h \mathbf{u}^{n+1}, \operatorname{div}_h \mathbf{v}_h) + g \int_\Omega \frac{D_{ij}(\mathbf{u}^{n+1})\, D_{ij}(\mathbf{v}_h)}{(D_{II}(\mathbf{u}^n) + \eta^2)^{1/2}} = \int \mathbf{f}_h \cdot \mathbf{v}_h\, d\Omega \qquad \text{for all} \quad \mathbf{v}_h \in V_h \tag{17}$$

We recall from [3] that the derivation of the stiffness matrices A, $B(\mathbf{u}_n)$ for $a(\mathbf{u}^{n+1}, \mathbf{v}_h)$ and $\hat{b}(\mathbf{u}^n, \mathbf{u}^{n+1}, \mathbf{v}_h)$ is carried out by 3×3 Gaussian quadrature. The stiffness matrix arising from the penalty term $(1/\epsilon)(\operatorname{div}_h \mathbf{u}^{n+1}, \operatorname{div}_h \mathbf{v}_h)$ is obtained by directly computing $(1/\epsilon) \int_\Omega (\operatorname{div} \mathbf{u}^{n+1})(\operatorname{div} \mathbf{v}_h)\, d\Omega$ by means of 2×2 Gaussian quadrature. The only new term here is the stiffness matrix $D(\mathbf{u}^n)$ for

$$\int_\Omega \frac{D_{ij}(\mathbf{u}^n)\, D_{ij}(\mathbf{v}_h)}{(D_{II}(\mathbf{u}^n) + \eta^2)^{1/2}}\, d\Omega.$$

Since the gradient of $D_{II}(\mathbf{u}^n)$ can be very large it is necessary to use a higher-order quadrature rule in order to follow the rapid changes in this nonlinear term. A 4×4 Gaussian quadrature rule was used and tests with 3×3 quadrature rule showed very poor convergence performance and in many cases oscillation and divergence.

Fortin [9], using a duality approach (Lagrange multiplier for the non-Newtonian term), observed the same phenomenon; that more refined approximation of the non-Newtonian term in the equations resulted in a more stable algorithm.

Thus the computation of the total stiffness matrix involves different quadrature rules for the different linear and nonlinear terms, the different choices for the quadrature order all being based on mathematical considerations. The pressure field P is "recovered" from the velocity field by evaluating $(1/\epsilon)\, \nabla \cdot \mathbf{u}$ at the 2×2 Gaussian points of integration, for each element; note that this results in a pressure field discontinuous at element boundaries. Algorithm (17) was applied using a value of $\eta = 10^{-14}$;

the machine accuracy for a CDC computer. It can be proved that for $g = 0$ (cf. [2]) the algorithm converges provided that Re is small enough. Unfortunately there are to date no theoretical results for $g > 0$ and this remains an area for futher research.

Numerical Results

Four different flows were studied:

(a) Wall-driven cavity. The boundary conditions are shown in Fig. 1a.

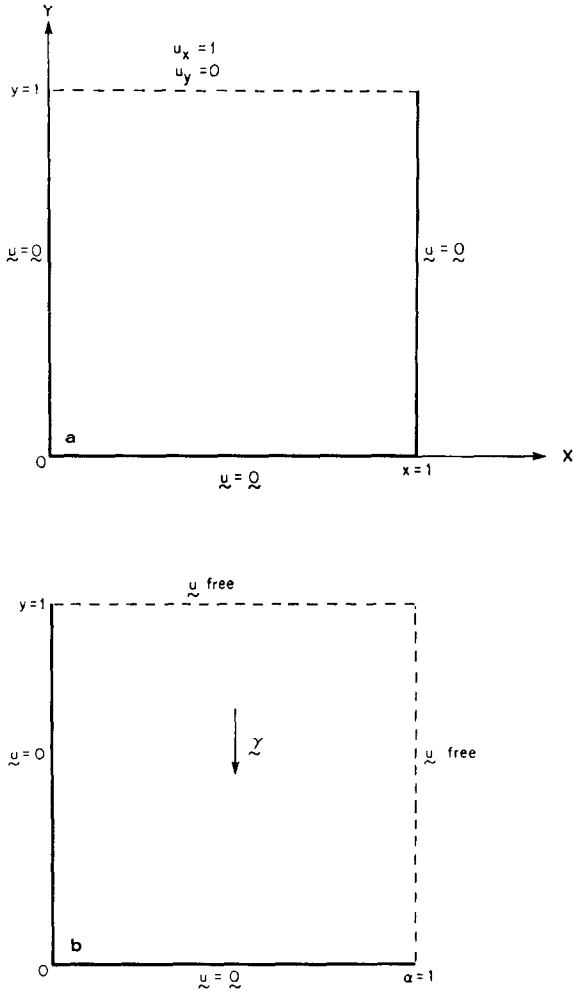

FIG. 1. (a) Wall-driven cavity, (b) limit load analysis.

(b) Fluid in a closed square cavity subject to the body force **F**:

$$F_{x_1} = 300(x_2 - \tfrac{1}{2}); \qquad F_{x_2} = -300(x_1 - \tfrac{1}{2})$$

with $\mathbf{u} = 0$ on the entire boundary.

(c) Fluid contained within two cylinders with the minor cylinder rotating with a constant angular speed such that for any point on the rotating boundary $u_0 = 1$.

(d) An application of Bingham fluids to the computation of the limit load for a von Mises plastic material. The boundary conditions are shown in Fig. 1b.

All numerical examples were run on the CDC Cyber 74 of the Hebrew University of Jerusalem Computer Centre. The rigid regions of the flows presented are depicted by crosses at those Gaussian points of integration (4 × 4) of an element for which the following condition holds:

$$D_{II}^{1/2} \leqslant h^2; \qquad h = \text{element dimension.} \tag{18}$$

Figure 2 is a contour plot of the function $D_{II}^{1/2}$ for 30 equally spaced values between 0. and 0.3 for the flow in a wall-driven cavity, $Re = 1$, $g = 7.5$ (Fig. 3c). The very sharp gradient in the region of $D_{II}^{1/2} = h^2$ is clearly evident and since the accuracy of the numerical technique is of $O(h^2)$, condition (18) is suitable for determining the rigid regions within the flow.

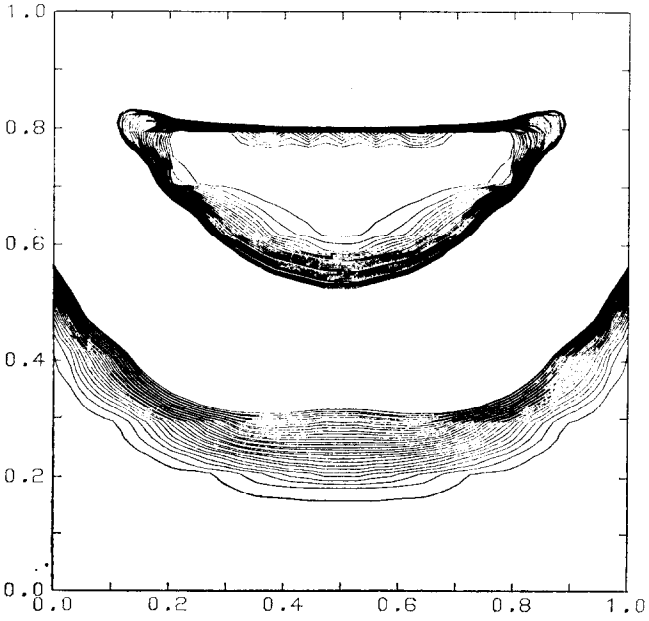

FIG. 2. Contour plot of SQRT (trace D ** 2).

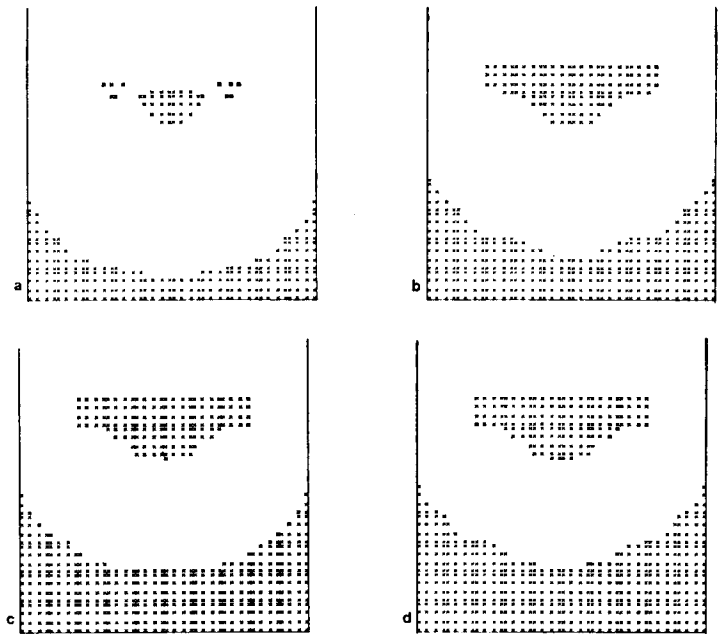

FIG. 3A. (a) Re = 1, g = 2.5. (b) Re = 1, g = 5. (c) Re = 1, g = 7.5. (d) Re = 1, g = 10.

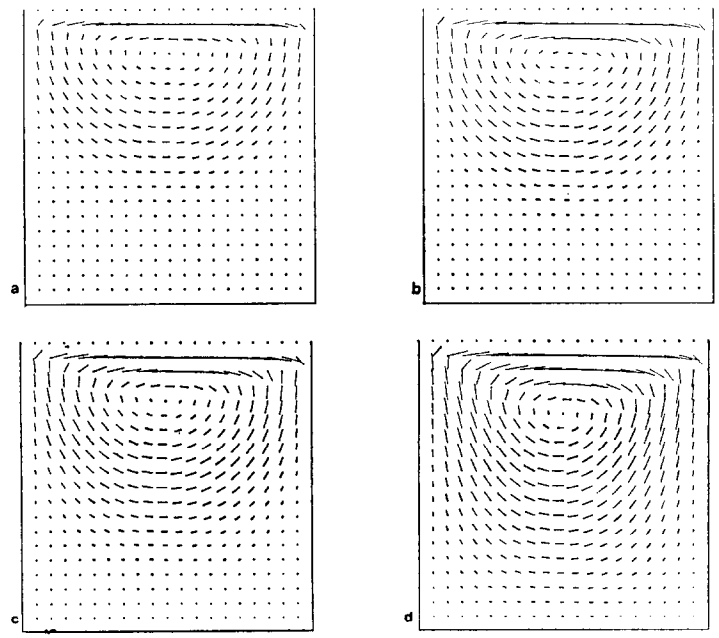

FIG. 3B. Wall-driven cavity—velocity vector plots. (a) Re = 1, g = 2.5. (b) Re = 1, g = 5. (c) Re = 1, g = 7.5. (d) Re = 1, g = 10.

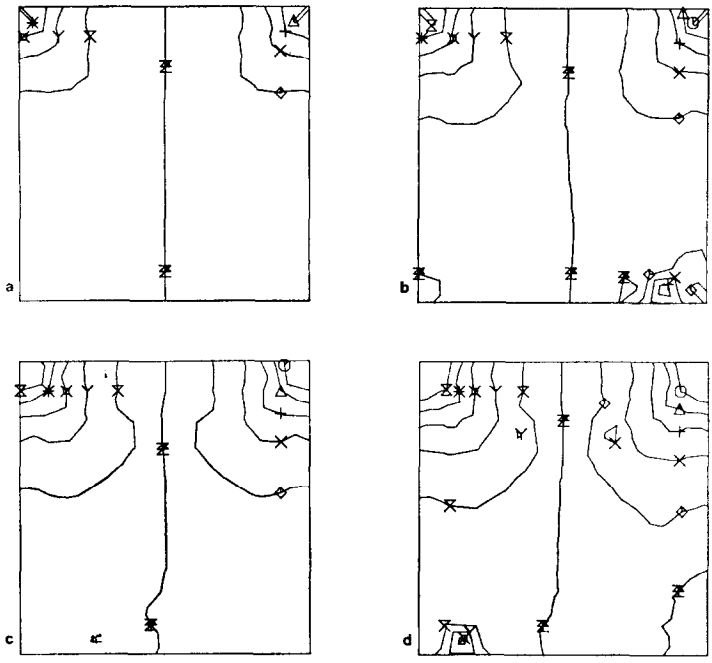

FIG. 3C. Wall-driven cavity—pressure contour plots. (a) Re = 1, $g = 2.5$. (b) Re = 1, $g = 5$. (c) Re = 1, $g = 7.5$. (d) Re = 1, $g = 10$.

Effect of Penalization Parameter ϵ

In order to establish the influence of the value of the penalization parameter ϵ,the cavity flow ($g = 5.$, $Re = 1$) was used. The same calculation was performed for $\epsilon = 10^{-2}, 10^{-3}, 10^{-4}, 10^{-5}, 10^{-6}, 10^{-7}$, the results being presented in Table I. These results illustrated the theoretical result, Eq. (15), which predicted an $O(\epsilon^{1/2})$ perturbation effect of the parameter ϵ as compared to the $O(\epsilon)$ effect for Newtonian fluids [3]. So that the effect will be less than the order of approximation, ϵ must be chosen smaller

TABLE I

Effect of Penalization Parameter ϵ

ϵ	Convergence behavior
10^{-2}	Rapid divergence
10^{-3}	No convergence
10^{-4}	Oscillatory slow convergence
10^{-5}	Convergence
10^{-6}	Convergence — no difference in number of iterations
10^{-7}	Convergence

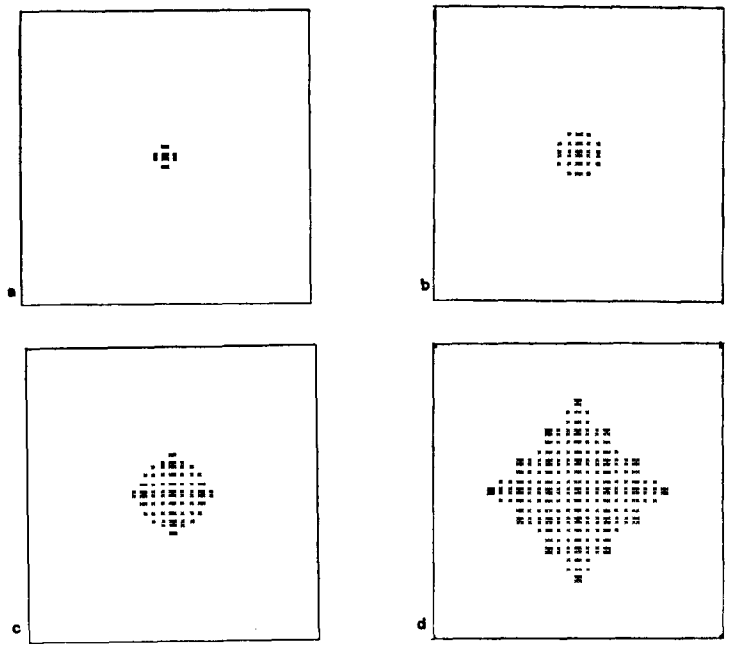

FIG. 4A. Body force problem—rigid regions. (a) $g = 5$. (b) $g = 7.5$. (c) $g = 10$. (d) $g = 15$.

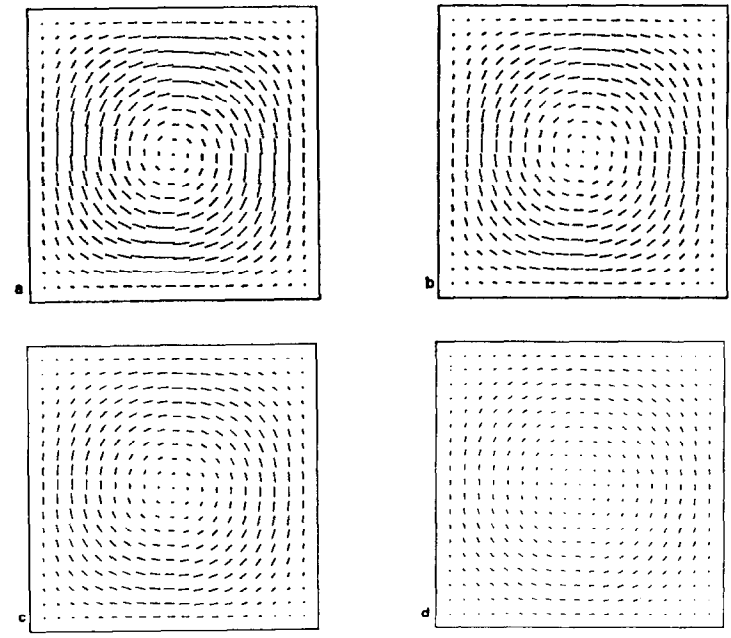

FIG. 4B. Body force problem—velocity vector plots. (a) $g = 5$. (b) $g = 7.5$. (c) $g = 10$. (d) $g = 15$.

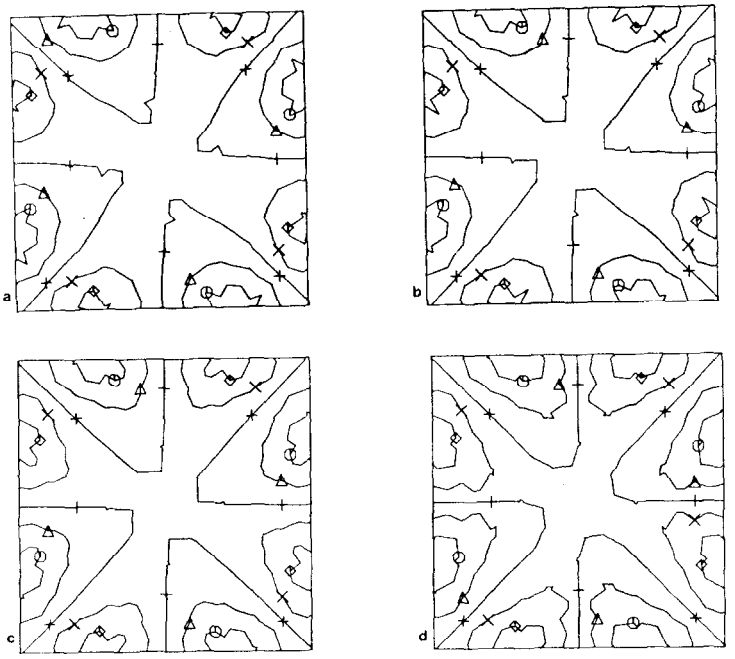

FIG. 4C. Body force problem—pressure contour plots. (a) $g = 5$. (b) $g = 7.5$. (c) $g = 10$. (d) $g = 15$.

than $O(h^2)$. All calculations presented in this paper were performed with a value of $\epsilon = 10^{-5}$.

Wall-Driven Cavity Flows

Computations were carried out for flows of $Re = 1.$ with $g = 2.5, 5., 7.5, 10.$ using a mesh of 10×10 square elements. The symmetry of these rigid regions, as compared to the results of Fortin [9] who used six-node triangles is clear, illustrating the advantages of quadrilaterials over triangles. The average number of iterations required to achieve a residue less than 10^{-4} was 25.

Figures 3A–C are the plots of the rigid regions, velocity vectors, and pressure contours for each of the four flows. In the pressure contour plots the different symbols represent the same pressure value in each plot.

Body Force Problem

Computations were performed for $Re = 1.$ with $g = 5., 7.5, 10., 15.$ rigid region, velocity vector, and pressure contour plots being presented in Figs. 4A–C, respectively. The heuristic prediction of the growth of the rigid region by Duvaut and Lions [5] is well illustrated by these results. It is interesting to note the appearance of rigid

regions in the four corners of the cavity for $g = 15$. Again the symmetry of the results is striking. In the pressure contour plots the $+$ line is the contour line of zero pressure. The other values are distributed equally about the zero value; $\bigcirc$ is 12, Δ is 6, $\times$ is -6 and $\diamond$ is -12 pressure units.

Rotating Flow

As an illustration of the effectiveness of the isoparametric element the flow between two cylinders, the minor rotating and the outer stationary, was calculated. Fig. 5b shows the rigid region of the flow and Fig. 5a the FEM mesh used for the calculation.

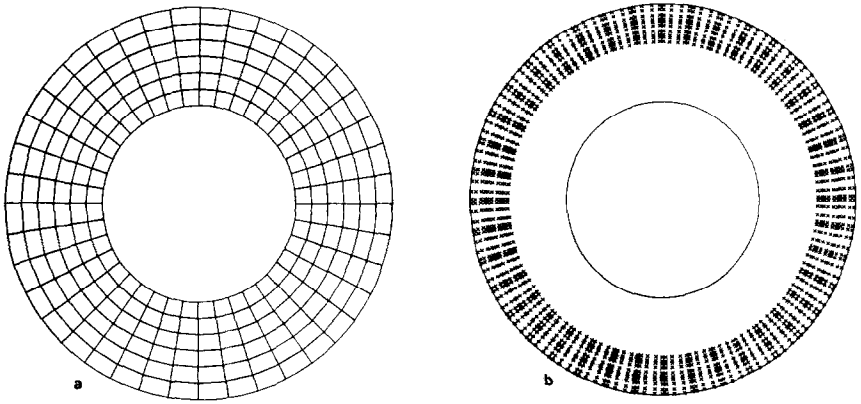

FIG. 5. Rotating flow between two cylinders. (a) FEM mesh. (b) Rigid region, $g = 5$, $w = 1$.

Limit Load Analysis of Mechanical Systems

Let the boundary Γ of Ω be given by $\Gamma = \Gamma_u \cup \Gamma_F$; then we consider the problem

$$\min_{\mathbf{v}} \left[\tfrac{1}{2}a(\mathbf{v}, \mathbf{v}) + g \int_\Omega D_{II}^{1/2}(\mathbf{v})\, d\Omega - sL(\mathbf{v})\right] \tag{19}$$

among all $\mathbf{v} \in (H^1(\Omega))^2$ such that $\operatorname{div} \mathbf{v} = 0$ and $\mathbf{v}|_{\Gamma_u} = 0$, where s is a scalar load multiplier and

$$L(\mathbf{v}) = \int_\Omega f_i v_i \, d\Omega + \int_{\Gamma_F} F_i v_i \, d\Gamma. \tag{20}$$

Duvaut and Lions [5] have shown that for a given $L(.)$ there exists a value S_c such that for all $S \leqslant S_c$ the solution of (19) is identically zero. By duality considerations Mercier [12] has proved that (19) can be used for the analysis of limit loads of systems made of "elasto-plastic" materials. In the plane strain analysis of a material of von Mises or Tresca type $g/2^{1/2}$ is the yield criterion and the limit analysis consists of finding S_c, where S_c is the load factor for which the mechanical system collapses. Most limit load analyses to date have been based on first-order finite elements. Here we apply the

nine-node element to the classic problem of the vertical earth cut, of Fig. 1b. Let $\gamma = (0, \gamma)$ be the gravitational force; H, the height of the cut; and $g/2^{1/2}$ the Tresca yield criterion. The problem of finding the limit load S_c can be restated as the dimensionless problem: find the smallest β, $\beta = H\gamma^{1/2}/g$, such that the solution of (19) is $\mathbf{u} = 0$. The problem has been dealt with in depth in [12, 4] and we refer the reader to these papers for full details. We have simulated the problem by setting $H = \gamma = 1$ and varying g.

Figures 6a–d are the regions of rigid flow for $g = 0.1, 0.2, 0.3, 0.385$. It can be seen that for $g = 0.385$ the flow is completely blocked. Additional runs in order to determine the exact value of g for completely blocked flow revealed that for $g = 0.38$ the

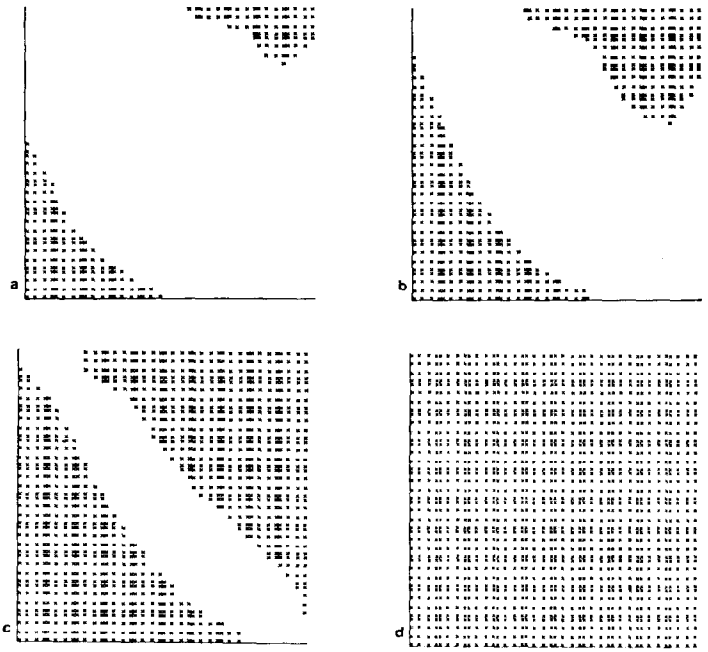

FIG. 6. Limit load analysis. (a) $g = 0.1$. (b) $g = 0.2$. (c) $g = 0.3$. (d) $g = 0.385$.

single Gaussian point of integration in the bottom right-hand corner was not rigid. Thus $\beta = 3.72$; this is to be compared with $\beta = 3.87$ as calculated by Mercier [12] and the classical theory prediction of $3.0 < \beta < 3.83$.

CONCLUSIONS

The penalty and reduced integration approach to the Navier–Stokes equations using a nine-node isoparametric element has been shown to be successful in the treatment of non-Newtonian fluid flows. The importance of the choice of the penalization

parameter ϵ and the use of a higher order of integration for the non-Newtonian term have been illustrated.

Although a rigorous proof of the convergence of the algorithm used and error estimates for the technique are still open questions at this stage, the quality of the results suggest that the method can have successful applications to practical problems. The program used for the numerical examples presented here, with the appropriate modifications to the constitutive relative, has been successfully used for the study of blood flows past artificial heart valves [8].

REFERENCES

1. D. BEGIS, Thèse de 3e cycle, Paris, 1972.
2. M. BERCOVIER, to appear.
3. M. BERCOVIER AND M. ENGELMAN, *J. Comput. Phys.* **30** (1979), 181.
4. J. M. DELBECQ, M. FREMOND, A. PECKER, AND J. SALENCON, *J. Méc. Appl.* **1**, No. 3 (1977).
5. G. DUVAUT AND J. L. LIONS, "Les inéquations en mécanique et en physique," Dunod, Paris, 1972.
6. M. ENGELMAN AND M. BERCOVIER, *C. R. Acad. Sci. Paris Sér. A* (12 Mars 1979), 555.
7. M. ENGELMAN, Thesis submitted for Ph. D., 1979.
8. M. ENGELMAN, S. MOSKOWITZ, AND J. BORMAN, *J. Thorac. Cardiovascular Surgery*, **19** (1980), 402.
9. M. FORTIN, Thèse d'état, Paris, 1972.
10. P. JAMET AND P. A. RAVIART, *in* "Méthodes de calcul scientifique et technique" (R. Glowinski and J. Lions, Eds.), Springer–Verlag, New York/Berlin, 1974.
11. O. A. LADYZHENSKAYA, "The Mathematical Theory of Viscous Incompressible Flows," Moscow, 1961. English translation, 2nd ed., Gordon & Breach, New York, 1969.
12. B. MERCIER, "Une méthode pour résoudre le problème des changes limites" *Journal de Mécanique* **16**, No. 3 (1977).
13. O. C. ZIENKIEWICZ AND P. N. GODBOLE, *in* "Finite Element Method in Flow Problems," Wiley, New York, 1975.